Monthly Notices of the ROYAL ASTRONOMICAL SOCIETY

MNRAS **534,** 1364–1375 (2024) https://doi.org/10.1093/mnras/stae2201
Advance Access publication 2024 September 23

ExoMol line lists–LIX. High-temperature line list for N_2O

Sergei N. Yurchenko, Thomas M. Mellor and Jonathan Tennyson ★
Department of Physics and Astronomy, University College London, Gower Street, WC1E 6BT London, UK

Accepted 2024 September 18. Received 2024 September 17; in original form 2024 June 3

ABSTRACT

New hot line lists for five isotopologues of N_2O called TYM are presented, for the parent $^{14}N_2{}^{16}O$ and 4 singly substituted species $^{14}N_2{}^{17}O$, $^{14}N_2{}^{18}O$, $^{14}N^{15}N^{16}O$ and $^{15}N^{14}N^{16}O$. The line lists have been computed with the variational program TROVE (Theoretical ROVibrational Energies) using a new empirical potential energy surface (PES) and an accurate *ab initio* dipole moment surface of N_2O Ames-1. The PES was obtained by fitting to experimentally derived energies of N_2O compiled using the well established measured active rotation vibration energy levels (MARVEL) procedure. Here we also introduce an 'artificial symmetry group' C_{ns}(AEM) for an efficient construction of rotation-vibrational basis set of a linear non-symmetric triatomic molecule of the XYZ type. The line lists cover the rotational excitations up to $J = 160$ and the wavenumber range up to 20000 cm^{-1}. MARVEL energies are also used to improve predicted line positions resulting in excellent agreement with the available experimental spectra, as demonstrated. An extensive comparison with existing line lists for N_2O HITRAN, HITEMP, NOSL-296, NOSD-1000, and Ames-296K is provided. The TYM line lists are freely accessible from www.exomol.com.

Key words: molecular data – opacity – exoplanets – planets and satellites: atmospheres – stars: atmospheres – ISM: molecules.

1 INTRODUCTION

N_2O (nitrous oxide) is a trace atmospheric species on Earth with notable spectral features (Sagan et al. 1993) and a dominantly biological origin. The emission of the 4.5 μm band of N_2O in the Earth atmosphere is known to be non-local thermodynamic equilibrium (non-LTE; López-Puertas et al. 2007). N_2O is therefore one of the molecules suggested as an observable bio-signature in Earth-like exoplanets (Grenfell 2017; Schwieterman et al. 2018, 2022). Its possible detection in exoplanets features strongly in telescope proposals (Tinetti et al. 2012; Angerhausen et al. 2024) and atmospheric models (Vasquez et al. 2013). Due to its atmospheric importance, there have been a wealth of experimental and theoretical studies on N_2O, see Tennyson et al. (2024) for a detailed review of the spectroscopic literature. N_2O has been detected in the interstellar medium (Ziurys et al. 1994), but as yet not in exoplanets.

Owing to the importance of N_2O for atmospheric studies, a number of nitrous oxide line lists for exist in the spectroscopic data bases. HITRAN 2020 (Gordon et al. 2022) provides an accurate spectroscopic data sets for multiple isotopologues of N_2O for (ambient temperature) terrestrial and planetary atmospheric applications based on the wealth of experimental data and targeting experimental accuracy. Its hih-temperature partner HITEMP (Rothman et al. 2010) provides hot line lists for N_2O isotopologues (Hargreaves et al. 2019) intended for high-temperature applications. HITEMP line lists aim to retain the accuracy of the lines in HITRAN by providing the completeness required at high temperatures. Another well-known N_2O line list family is produced and maintained by the laboratories in Tomsk, a high-accuracy, low-temperature line list NOSL-296 (Tashkun & Campargue 2023) and its high-temperature partner NOSD-1000 (Tashkun, Perevalov & Lavrentieva 2016). All four line lists are empirical in nature produced using effective Hamiltonian and dipole moment models. They typically provide line positions, line intensities ($T = 296$ K or 1000 K), Einstein coefficients, lower state energies, line broadening parameters (except NOSL-296) and line shifts (except NOSD-1000 and NOSL-296) parameters and are equipped with associated quantum numbers.

Recently, Huang, Schwenke & Lee (2023) produced room temperature line lists for N_2O isotopologues Ames-296K using an accurate empirical potential energy surface (PES) Ames-1 and a high level *ab initio* dipole moment surface (DMS) Ames-1. This line list is different from the effective models as it is based on the so-called 'Best Theory + Reliable High-Resolution experiment' strategy (Huang, Schwenke & Lee 2021), where the variational methods are used to solve the nuclear motion Schrödinger equation. The empirical PESs are obtained by fitting to experimental energies/line positions and high level *ab initio* DMS are used in intensity calculations.

In this work, we follow a similar variational methodology and report empirical line lists for five isotopologues of N_2O, including the parent $^{14}N_2{}^{16}O$ and four singly substituted species $^{14}N_2{}^{17}O$, $^{14}N_2{}^{18}O$, $^{14}N^{15}N^{16}O$, and $^{15}N^{14}N^{16}O$, valid up to 2000 K. The line lists cover the wavenumber range up to 20000 cm^{-1} and rotational excitations up to $J = 160$. The variational program TROVE (Theoretical ROVibrational Energies, Yurchenko, Thiel & Jensen 2007) is used to solve the Schrödinger equation for the nuclear motion of N_2O and to compute the ro-vibrational energies and wavefunctions. For the intensities a high level *ab initio* DMS reported by Huang et al. (2023) is used. The production of the line lists is heavily based on the recently reported experimentally energies of $^{14}N_2{}^{16}O$ (Tennyson et al. 2024) derived using the MARVEL (measured active rotation vibration energy levels) procedure of Furtenbacher, Császár

★ E-mail: j.tennyson@ucl.ac.uk

Table 1. Character table for the C_{4s}(AEM) group. The operations of the group that are 0-superscripted correspond to the C_s group. Note that the characters of the 0-superscripted irreps for these operations are the same as those of the corresponding irreps for the C_s group.

C_{4s}(AEM)	C_s	E^0	σ^0	E^1	σ^1	E^2	σ^2	E^3	σ^3
A'_0	A'	1	1	1	1	1	1	1	1
A''_0	A''	1	−1	1	−1	1	−1	1	−1
A'_1	–	1	1	−1	−1	1	1	−1	−1
A''_1	–	1	−1	−1	1	1	−1	−1	1
A'_2	–	1	1	1	1	−1	−1	−1	−1
A''_2	–	1	−1	1	−1	−1	1	−1	1
A'_3	–	1	1	−1	−1	−1	−1	1	1
A''_3	–	1	−1	−1	1	−1	1	1	−1

& Tennyson (2007); these empirical energy levels are used to refine an *ab initio* PES of Schröder et al. (2015). The line list for the parent isotopologue is improved by substituting the calculated ro-vibrational energies with experimentally derived values by Tennyson et al. (2024) where available.

2 VARIATIONAL NUCLEAR MOTION CALCULATIONS

For the variational calculations, we used an exact kinetic energy operator (KEO) with a bisector frame as implemented in TROVE in combination with the associated Laguerre polynomials as reported by Yurchenko & Mellor (2020). The TROVE computational protocol consists of four steps, described in detail below. Nuclear masses were used: $m_N = 13.999233945$ Da (^{14}N) and 14.99626884 Da (^{15}N); $m_O = 15.990525980$ (^{16}O), 16.99474312 Da (^{17}O), and 17.99477097 Da (^{18}O).

Step 1. The primitive vibrational basis set is comprised of three types of one-dimensional basis functions. For the stretching modes N–O and N–N, two 1D vibrational Schrödinger equations were solved using the Numerov–Cooley method (Noumerov 1924; Cooley 1961) for 1D Hamiltonians constructed by freezing two other vibrational modes except the one in question. For the N–N and N–O stretching basis functions $\phi_{v_1}(r_1)$ and $\phi_{v_2}(r_2)$, respectively, grids of 2000 and 3000 points were used, ranging between $[-0.3, 0.90]$ Å and $[-0.4, 0.75]$ Å around the corresponding equilibrium values 1.1282021 and 1.1845554 Å, respectively. For the bending mode N–N–O basis set $\phi_{v_3}^{(L)}(\rho)$, a similar 1D Hamiltonian was constructed and variationally solved using the associated Laguerre polynomials on a grid of 12000 points of $\rho = [0, \rho_{\max}]$, where L is the vibrational angular momentum index defined as $0 \le L \le v_3$ and $\rho_{\max}$ was set to 120°.

The (exact) KEO is constructed numerically as a formal expansion in terms of the inverse powers of the stretching coordinates r_i ($i = 1, 2$): $1/r_i$ and $1/r_i^2$ around a non-rigid configuration (Hougen, Bunker & Johns 1970) defined by the ρ_i points on the grid. The singularities of the KEO at $\rho = 0°$ ($\sim 1/\rho$ and $1/\rho^2$) are resolved analytically with the help of the factors $\rho^{L+1/2}$ in the definition of the associated Laguerre basis set. The details of the KEO and the matrix elements involved are given by Yurchenko & Mellor (2020).

Step 2. The individual 1D vibrational basis functions are then assigned to an irreducible representation (irrep) for the symmetry group chosen. Here we implemented and used the so-called artificial symmetry group C_{ns}(AEM) with a procedure analogous to the one described by Mellor, Yurchenko & Jensen (2021) but for the case of a non-symmetric molecule.

The artificial symmetry group C_{ns}(AEM) consists of one-dimensional, real irreps, each of which is correlated with the vibrational index L. From C_{ns}(AEM) we select two elements and match each with a C_s element. The irreps of C_{ns}(AEM) are labelled as $\Gamma = A'$ and A'' irreps with an extra subscript (see Table 1), e.g. A'_4. For example, a vibrational function with $l = 4$ and transforming as A' in C_s would be assigned the symmetry A'_4 in the C_{ns}(AEM). The 0-superscripted irreps are the only physical irreps, matched to A' and A'' of C_s together with the corresponding characters of each element, while all irreps of $l > 0$ are non-physical, i.e. 'artificial'. The full description of this case is given below, for the first time.

A 3D vibrational (L-dependent) basis set for the $J = 0$ Hamiltonian is formed for each $L \le L_{\max}$ as symmetry adapted products given by:

$$\Phi^{\Gamma_{\rm vib}}_{v_1,v_2,v_3,L} = \{\Phi_{v_1}(r_1) \times \Phi_{v_2}(r_2) \times \Phi_{v_3,L}(\rho)\}^{\Gamma_{\rm vib}}, \quad (1)$$

where $\Gamma_{\rm vib}$ is the vibrational symmetry in C_{ns}(AEM) and will be that of the $\Phi_{v_3,L}(\rho)$. This is because the function as the irreps of ϕ_{i_1} and ϕ_{i_2} are A'_0, so have no impact of the irrep of the combined vibrational function. Thus, the symmetry of the vibrational basis function $\Phi^{\Gamma_{\rm vib}}_{v_1,v_2,v_3,L}$ is wholly classified by the corresponding value of L. The total vibrational basis set is the subject to the cutoff based on the following truncation scheme,

$$3v_1 + \frac{3}{2}v_2 + v_3 \le 48. \quad (2)$$

The vibrational $J = 0$ eigen-solutions $\Psi^{(J=0,\Gamma_{\rm vib})}_{\lambda,L}$ are found for a range of values of $L = 0 \ldots L_{\max}$ by solving for the $J = 0$ Hamiltonian $\hat{H}^{(J=0)}$, for all corresponding irreps A'_L or A''_L covering available for $L_{\max}$, where we used $L_{\max} = 18$.

Step 3. The final ro-vibrational basis set for $J > 0$ calculations is then formed as a contracted, symmetrized product of the $J = 0$ vibrational functions:

$$\Psi^{(J,\Gamma)}_{\lambda,K} = \{\Psi^{(J=0,\Gamma_{\rm vib})}_{\lambda,K} |J, K, \Gamma_{\rm rot}\rangle\}^{\Gamma}, \quad (3)$$

where the rotational part $|J, K, \Gamma_{\rm rot}\rangle$ is a symmetrized combination of the rigid rotor functions (Yurchenko, Yachmenev & Ovsyannikov 2017) and the rotational quantum number K ($K \ge 0$) is constrained to the vibrational parameter L ($K = L$) with the the rotational irrep $\Gamma_{\rm rot}$ defined as

$$\Gamma_{\rm rot} = A'_{2K+1}, \ \tau_{\rm rot} = 0 \quad (4)$$

$$\Gamma_{\rm rot} = A''_{2K+2}, \ \tau_{\rm rot} = 1, \quad (5)$$

where $\tau_{\rm rot}$ is the parity of the Wang-type rotational basis function $|J, K, \tau_{\rm rot}\rangle$ (Yurchenko et al. 2017). Here Γ, $\Gamma_{\rm vib}$, and $\Gamma_{\rm rot}$ are the total, vibrational and rotational symmetries in C_{ns}(AEM), $K = |k| = L$, k and m is the projection of the angular momentum on the molecular z and laboratory Z axes, respectively, and $i_{\rm vib}$ is a TROVE vibrational index to count the $\Phi^{J=0,K,\Gamma_{\rm vib}}_{i_{\rm vib}}$ functions regardless of their symmetry, see Yurchenko et al. (2017).

Table 2. Line lists of N_2O isotopologues: number of entries and statistical weights used; also given in the shorthand name for each isotopologue used by HITRAN which based on the last digit of the atomic number of each atom. The corresponding nuclear statistical weights g_{ns} for each isotopologues are also listed.

Molecule	Shorthand	g_{ns}	N_{states}	N_{trans}
$^{14}N_2{}^{16}O$	446	9	2078676	1532806222
$^{14}N_2{}^{17}O$	447	54	2150170	1620106701
$^{14}N_2{}^{18}O$	448	9	2216809	1705390240
$^{14}N^{15}N^{16}O$	456	6	2183803	1856305463
$^{15}N^{14}N^{16}O$	546	6	2171200	1667908595

When these are combined, the symmetry of the resultant function is 0-subscripted only if the subscripts of the bending and rotational functions are the same. If not, then the subscript is not 0. Moreover, the symmetry of the combined function corresponds to the C_s symmetry – in the sense established above – and thus, ignoring the subscript, is the same symmetry had we worked solely in the C_s group. For example, $A'_3 \otimes A''_3$ is A''_0 while $A''_3 \otimes A''_1$ is A'_2.

Step 4: Intensity calculations. The variational wavefunctions computed at Step 3 are then used to compute ro-vibrational line strengths of N_2O for transitions up to J_{max} between all states satisfying the electric dipole selections rules

$$\Delta J = 0, \pm 1 \tag{6}$$

$$J' + J'' \neq 0, \tag{7}$$

$$A' \leftrightarrow A''. \tag{8}$$

Here A' and A'' have the standard correlation rules with the spectroscopic parities e and f as follows: the parity of $\Gamma = A'$ and A'', 1 and -1, respectively, correspond to $(-1)^J$ for e and $(-1)^{J+1}$ for f. The lower and upper states were limited by the energy thresholds of 10000 cm^{-1} and 24000 cm^{-1}, respectively. The range of transition wavenumbers is 0 to 20000 cm^{-1}. The artificial symmetry states A'_k and A''_k ($k > 0$) must be excluded from the intensity calculations. In TROVE, this can be done by setting the corresponding statistical weight factors g_{ns} to zero, similar to how the non-physical states were excluded in the HOOH calculations using the extended symmetry group D_{2h}(EM) by Al-Refaie et al. (2016) or by simply not computing these states on the first place. The nuclear statistical weights g_{ns} of the physical states of the isotopologues considered are listed in Table 2. A detailed description of the procedure to construct the C_{ns}(AEM) irreps is given in Appendix A.

The main advantage of C_{ns}(AEM) is that it permits us to use the efficient machinery of irreducible representations implemented in TROVE (Yurchenko et al. 2017) to construct the L-dependent vibrational basis and also to combine it with the rotational K-dependent basis functions. In this way, the non-standard basis set (for TROVE) is exploited by the same generalized TROVE implementation (with only some minimal changes) used for any other, more standard basis sets. This is in contrast to an overhaul of the program which may otherwise have been required.

2.1 Quantum numbers

The computed TROVE ro-vibrational energies are assigned by the two rigorous quantum 'numbers', J, the rotational angular momentum quantum number, and the total symmetry Γ in C_{ns}(AEM) and also identified by the eigen-state counting number λ (in the order of increasing energies). In order to help in spectroscopic applications, we also use approximate quantum numbers (QN) associated with the corresponding largest basis set contributions (Yurchenko et al. 2007). This provides a measure for how close the variationally computed wavefunctions are to the rotational and vibrational basis set used. The vibrational TROVE QNs are associated with the primitive basis set excitation numbers v_1, v_2, v_3, and L (see the description of the vibrational basis set above). Remember that the rotational quantum number K is constrained to the value of L. These 'local' mode quantum numbers are approximately correlated to the spectroscopic, normal mode quantum numbers n_1, n_2^{lin}, n_3 of N_2O as follows:

$$n_1 = v_1 \,(\mathrm{NO}) \tag{9}$$

$$n_3 = v_3 \,(\mathrm{NN}) \tag{10}$$

$$n_2^{lin} = 2v_3 + L, \,(\mathrm{NNO}) \tag{11}$$

with L defined the same way in both conventions. According to the normal mode convention, also used by HITRAN, n_1 and n_3 are two stretching quantum numbers associated with the NO and NN modes, respectively; n_2^{lin} is the linear molecule bending quantum number; n_2^{lin} and L are two bending quantum numbers satisfying the standard condition on the vibrational angular momentum of an isotropic 2D Harmonic oscillator (Bunker & Jensen 1998)

$$L = n_2^{lin}, n_2^{lin} - 2, \ldots 1(0).$$

Following recent spectroscopic recommendations for the quantum numbers of nitrous oxide (Teffo, Perevalov & Lyulin 1994; Waalkens, Jung & Taylor 2002; Tennyson et al. 2024), we also add the polyad quantum number scheme, (P, N), with the polyad number P given by

$$P = 2n_1 + n_2^{lin} + 4n_3 \tag{12}$$

and N is the polyad counting number within the same P, J, and Γ. This scheme has been shown to be more practical for description of nitrous oxide spectra characterized with many resonances among the excited vibrational states.

2.2 Potential energy surface and empirical refinement

The PES of N_2O was originally taken from the *ab initio* study of Schröder et al. (2015), which we then converted to the Morse type expansion as the form more comfortable for TROVE. We also made sure the expansion point was taken exactly at the minimum. The PES was expressed analytically by an expansion

$$V = \sum_{ijklmn} f_{ijk} \xi_1^i \xi_2^j \xi_3^k + V_{N_1O}, \tag{13}$$

in terms of

$$\xi_1 = 1 - \exp[-b_1(r_{NN} - r_{NN}^e)], \tag{14}$$

$$\xi_2 = 1 - \exp[-b_2(r_{NO} - r_{NO}^e)], \tag{15}$$

$$\xi_3 = \sin\rho = \sin(\alpha). \tag{16}$$

Here, r_{NN} and r_{NO} are the bond lengths and α is the bond angle. In equation (13), f_{ijklmn} are the expansion parameters with maximum expansion order $i + j + k = 8$ with the linear expansion parameters fixed to zero and

$$V_{N_1O} = b_1 \exp(-g_1 r_{N_1O}) + b_2 \exp(-g_2 r_{N_1O}^2)$$

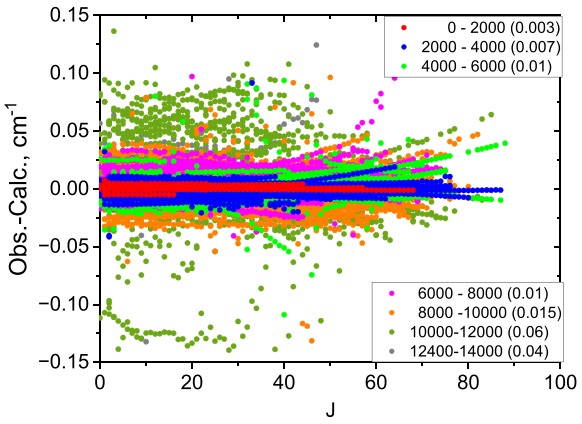

Figure 1. Fitting residual errors (obs.-calc.), i.e. the energy difference (in cm^{-1}) of N_2O between the empirically-derived MARVEL energies and computed TROVE values, as a function of the total angular momentum quantum number J. Different colours indicate corresponding energy ranges (cm^{-1}). The number in parentheses indicate the corresponding values of root-means-square error cm^{-1} evaluated for the given energy range.

is to ensure that the PES behaves correctly when the distance between the outer N and O atoms,

$$r_{N_1O} = \sqrt{r_{NN}^2 + r_{NO}^2 - 2r_{NN}r_{NO}\cos\alpha}, \quad (17)$$

becomes small. The parameters b_1, b_2, g_1, and g_2 were set to numerical values taken from Tyuterev, Tashkun & Schwenke (2001; see the expansion parameter list of the PES in the supplementary material).

The '*ab initio*' expansion parameters f_{ijklmn} are then refined by fitting to the N_2O MARVEL energies for $J = 0$, 1, 2, 3, 4, 5, 8, 10, 15, 18, 20, 23, 25, 28, 30, 33, 35, 38, 40, 43, 45, 50, 55, 60, 65, 70, 75, 80 (6563 in total). The PES was constrained to the *ab initio* PES of Schröder et al. (2015) in the fitting – in order ensure the refined PES maintained a realistic shape. The quality of the fit is demonstrated in Fig. 1, where the fitting residuals are plotted as the obs.-calc. differences (in cm^{-1}) between the MARVEL and computed TROVE N_2O term values. The total root-mean-square error for all 17532 MARVEL energies ranging from $J = 0$ to $J = 88$ is 0.02 cm^{-1} which can be broken down to 0.003, 0.007, 0.01, 0.01, 0.025, 0.06, and 0.04 cm^{-1} for 7 consecutive 2000 cm^{-1} energy windows, 0–2000, 2000–4000 ,..., 12000–14000 cm^{-1}, respectively, as shown in detail in Fig. 1. A full list of the observed (MARVEL) versus calculated (TROVE) energies is given as supplementary material A Fortran 95 subroutine of the PES with the associated potential parameters is also provided as part of in the supporting information.

Table 3. Extract from the transitions file for the TYM line list for $^{14}N_2{}^{16}O$.

f	i	A_{fi}
1231756	1225215	1.4846e-02
793179	769026	2.0204e-04
163131	190123	2.3858e-07
1104614	1123948	3.5531e-03
398656	406929	5.4400e-14
958126	936653	1.9693e-06
564414	538184	4.7135e-04
309652	335938	2.3277e-15
1084933	1077737	3.1981e-06
744643	721037	5.4061e-05

Notes. f: upper state counting number.
i: lower state counting number.
A_{fi}: Einstein-A coefficient in s^{-1}.

Table 4. Extract from the `.states` file of the $^{14}N_2{}^{16}O$ TYM line list.

i	$\tilde{E}$/cm^{-1}	g	J	unc./cm^{-1}	τ / s^{-1}	Γ_{tot}	n_1	n_2^{lin}	L	n_3	P	N	v_1^T	v_2^T	v_3^T	Ca/Ma	$\tilde{E}_T$/cm^{-1}
90879	1330.799312	189	10	0.082640	8.2640E-02	A'	1	0	0	0	2	2	0	1	0	Ma	1330.796620
90880	1795.216842	189	10	0.917890	9.1789E-01	A'	0	3	1	0	3	1	0	0	1	Ma	1795.212483
90881	1813.184239	189	10	2.082000	2.0820E+00	A'	0	3	3	0	3	1	0	0	0	Ma	1813.184066
90882	1926.184734	189	10	0.080722	8.0722E-02	A'	1	1	1	0	3	2	0	1	0	Ma	1926.189641
90883	2269.466170	189	10	0.004612	4.6116E-03	A'	0	0	0	1	4	1	1	0	0	Ma	2269.470737
90884	2368.836444	189	10	0.558110	5.5811E-01	A'	0	4	0	0	4	2	0	0	2	Ma	2368.841085
90885	2377.406604	189	10	0.728660	7.2866E-01	A'	0	4	2	0	4	1	0	0	1	Ma	2377.406507
90886	2402.591231	189	10	1.577900	1.5779E+00	A'	0	4	4	0	4	4	0	0	0	Ca	2402.591231
90887	2507.989605	189	10	0.068005	6.8005E-02	A'	1	2	0	0	4	3	0	1	1	Ma	2507.992379
90888	2520.835439	189	10	0.078324	7.8324E-02	A'	1	2	2	0	4	2	0	1	0	Ma	2520.842253
90889	2609.053987	189	10	0.033480	3.3480E-02	A'	2	0	0	0	4	4	0	2	0	Ma	2609.054662

i: state counting number.
$\tilde{E}$: state energy in cm^{-1}.
g_{tot}: total state degeneracy.
J: total angular momentum.
unc.: Uncertainty cm^{-1}.
τ: life time in s.
Γ: total symmetry index in C_s(M)
n_1: normal mode stretching N-N quantum number.
n_2^{lin}: normal mode bending quantum number.
L: normal mode vibrational angular momentum quantum number.
n_3: normal mode stretching N-O quantum number.
P: polyad number $P = 2n_1 + n_2^{lin} + 4n_3$.
N: polyad counting number.
v_1^T: TROVE stretching vibrational quantum number.
v_2^T: TROVE stretching vibrational quantum number. v_3^T: TROVE bending vibrational quantum number.
Label: 'Ma' for MARVEL, 'Ca' for calculated.
Calc: original TROVE calculated state energy (in cm^{-1}).

Table 5. Extract from the .states file of the $^{15}N^{14}N^{16}O$ TYM line list.

i	$\tilde{E}$/cm^{-1}	g	J	unc./cm^{-1}	τ / s^{-1}	Γ_{tot}	P	L	N	v_1^T	v_2^T	v_3^T
1	0.000000	6	0	0.000000	Inf	A'	0	0	1	0	0	0
2	1159.969926	6	0	0.004000	1.2952E+00	A'	2	0	1	0	0	1
3	1269.827291	6	0	0.002000	9.2669E-02	A'	2	0	2	0	1	0
4	2201.624173	6	0	0.002000	4.6657E-03	A'	4	0	1	1	0	0
5	2305.159703	6	0	0.008000	5.2771E-01	A'	4	0	2	0	0	2
6	2439.580951	6	0	0.006000	7.3000E-02	A'	4	0	3	0	1	1
7	2534.448361	6	0	0.004000	3.7802E-02	A'	6	0	1	0	2	0
8	3333.728378	6	0	0.006000	4.9171E-03	A'	6	0	2	1	0	1
9	3439.341846	6	0	0.012000	2.7835E-01	A'	6	0	3	0	0	3

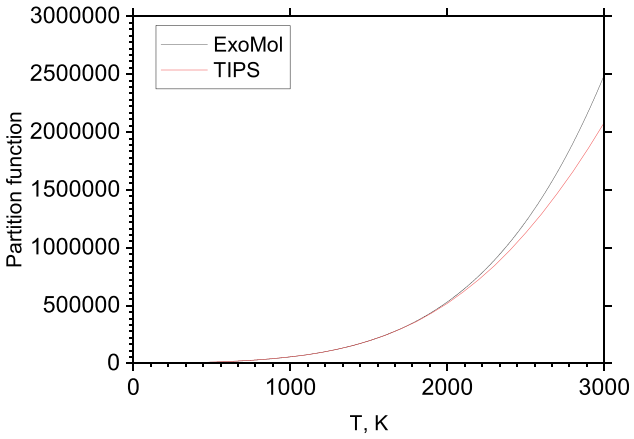

Figure 2. Temperature-dependence of the partition function $Q(T)$ of $^{14}N_2{}^{16}O$ computed using the TYM line list and compared to the TIPS values (Gamache et al. 2021).

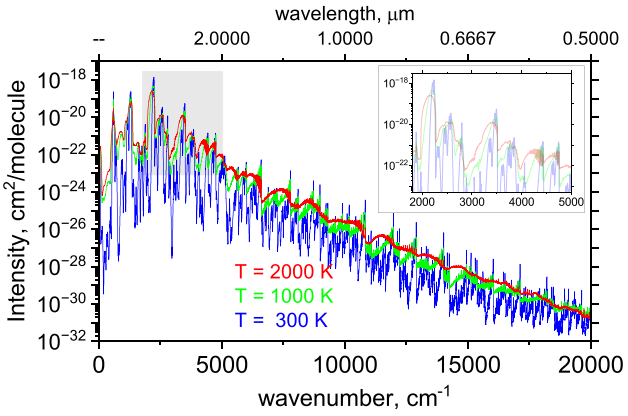

Figure 3. An overview of the absorption spectrum of N_2O at three temperatures computed using TYM with ExoCross and assuming the Gaussian line profile of half width-half-maximum (HWHM) of 1 cm^{-1}. The inset shows an enlarged part of the IR spectrum.

2.3 Dipole moment surfaces and uncertainties of intensities

In the line list production, the intensity were computed using the most recent, high-level of theory [CCSD(T)/aug-cc-pV(T,Q,5)Z extrapolated to one electron basis set limit] *ab initio* DMS of Huang et al. (2023). It has been demonstrated to provide high-quality intensities of N_2O isotopologues. This DMS is analytically represented using the pseudo-charge form (Huang et al. 2014) via its projections to the molecular bonds and therefore needs to be rotated to the bisector frame used in TROVE ro-vibrational calculations. This is done on the fly at each bending grid point ρ_k by re-expanding it in terms of the stretching displacement Δr_{NN} and Δr_{NO} around the equilibrium geometry (see above) in the polynomials of the 12th order using the finite differences and employing the quadrupole-precision (see Yurchenko et al. 2007).

3 THE N_2O TYM LINE LIST

3.1 Line list structure

Using the methodology described, line lists, called TYM, for five isotopologues of N_2O were computed. They cover the 0 to 20000 cm^{-1} range for ro-vibrational states with rotational excitation up to $J = 160$. The lower and upper state energy thresholds were chosen to be 10000 and 24000 cm^{-1}, respectively. The parent istopologue is represented by 1532 806 222 transitions between 2078 676 states. The transitions are divided into 1000 cm^{-1} wavenumber ranges to make them more manageable. Table 2 lists numbers of states and transitions in line lists of five N_2O isotopologues as well as the nuclear-spin degeneracy g_{ns}; note our partition functions include the full nuclear spin degeneracy.

The line lists is provided in the ExoMol data format (Tennyson, Hill & Yurchenko 2013). An extract from one of the `.trans` transition files of $^{14}N_2{}^{16}O$ is shown in Table 3. They contain upper and lower state ID numbers along with the Einstein A coefficient (in s^{-1}) of the transition between the states. An extract from the `.states` states file of $^{14}N_2{}^{16}O$ is given in Table 4, respectively; it contains a list of the ro-vibrational states with state ID numbers, energies (in cm^{-1}), uncertainties (in cm^{-1}), state lifetimes and quantum numbers. We use the standard spectroscopic normal mode quantum numbers in the `.states` file but also keep the TROVE quantum numbers for traceability. The mapping between the two sets is discussed in Section 2.1. In contrast to the rigorous quantum numbers J and Γ (irrep), the non-rigorous quantum numbers n_1, n_2^{lin}, n_3 and even $L = K$ are approximate and are defined using the largest eigencontribution approach. As a note of warning, this procedure cannot guarantee comprehensive quantum number descriptions with unique and unambiguous labels thus serving more as a measure of the main character of the state in question.

The `.states` file for $^{14}N_2{}^{16}O$ is also 'MARVELized', i.e. the TROVE energies are replaced with the empirical (MARVEL) energies from Tennyson et al. (2024) where available. The uncertainties are defined either as the MARVEL uncertainty if available, or for calculated levels estimated as (in cm^{-1}):

$$\text{unc} = 0.002(n_1 + n_2 + n_3) + 0.00002J(J+1), \quad (18)$$

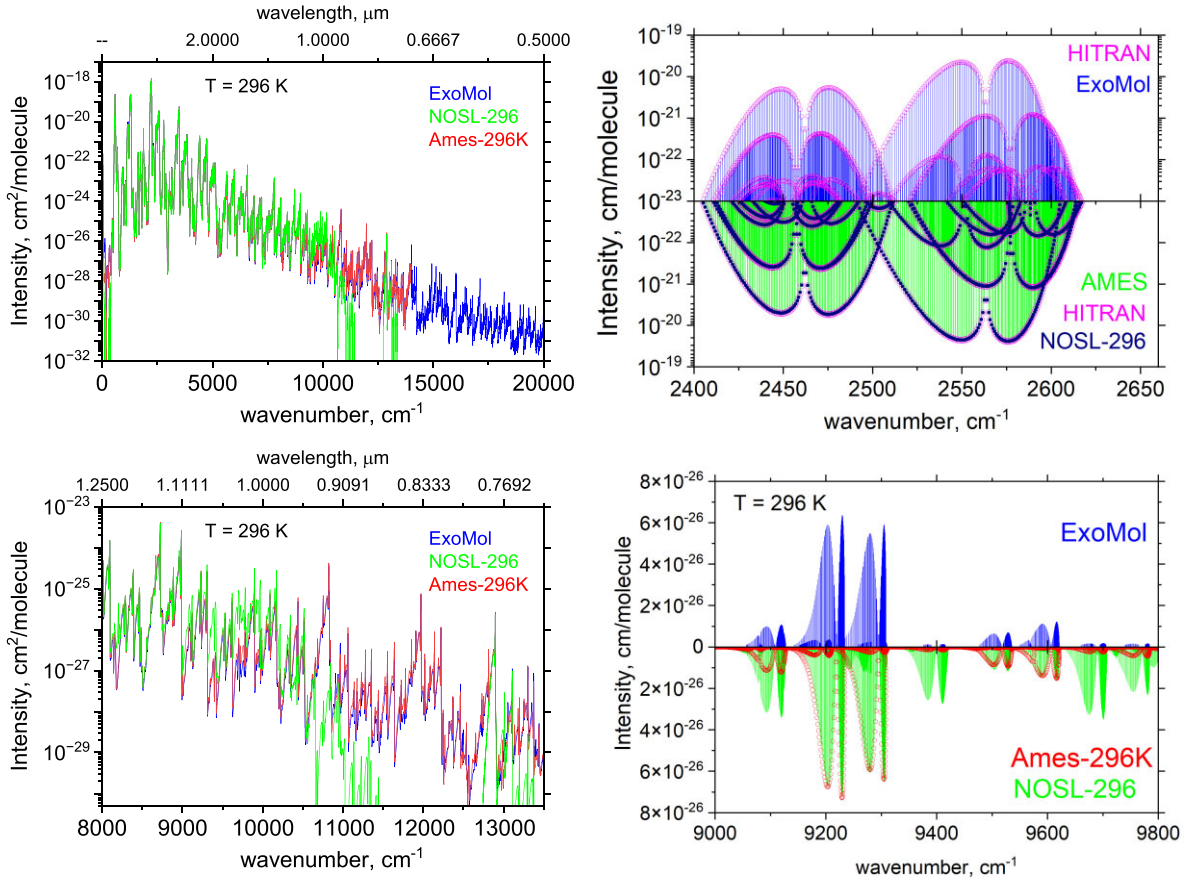

Figure 4. Comparison of $^{14}N_2{}^{16}O$ $T = 296$ K spectra computed using four line lists, TYM (ExoMol), HITRAN 2020 (Gordon et al. 2022), NOSL-296 (Tashkun & Campargue 2023), and Ames-296K (Huang et al. 2023). Left display: a log-scale illustration of the coverage of TYM (ExoMol), Ames-296K, and NOSL-296 using a Gaussian line profile with HWHM of 1 cm^{-1} . Right display: absorption coefficients (also in log-scale) of $^{14}N_2{}^{16}O$ in the 2400–2650 cm^{-1} wavenumber window of HITRAN (empty circles), NOSL-296 (circles), Ames-296K (sticks), and TYM (sticks). An extended comparison is provided in the Appendix B.

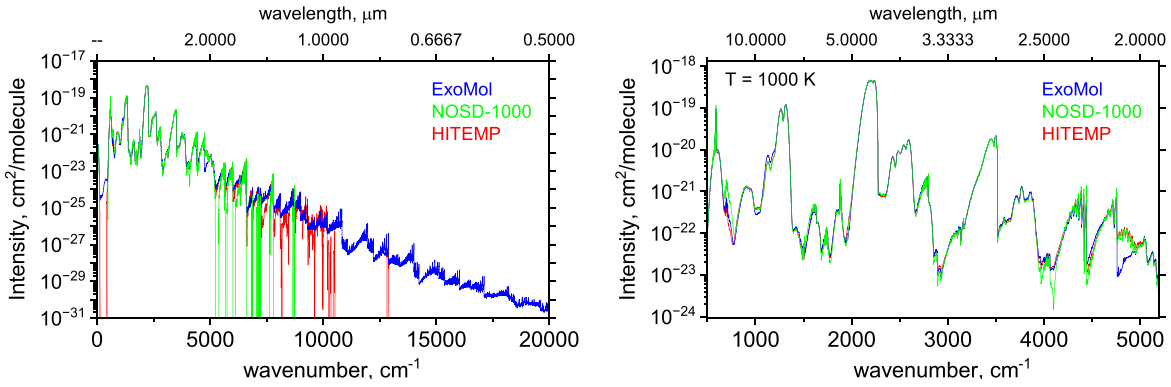

Figure 5. Comparison of hot ($T = 1000$ K) spectra of $^{14}N_2{}^{16}O$ computed using three line lists, TYM (ExoMol), N_2O HITEMP (Hargreaves et al. 2019) and NOSD-1000 (Tashkun et al. 2016), for the full range of 0–20000 cm^{-1} (left display) and for a smaller window of 500–5200 cm^{-1}.

where n_1–n_3 are the TROVE normal mode quantum numbers. These uncertainties are only approximate and designed to grow steadily with increasing rotational and vibrational excitation, where we tend to be conservative in estimating values for highly excited states.

In the case of the minor isotopologues, we could not establish a solid correlation between the spectroscopic normal mode and TROVE's local mode quantum numbers. We therefore retain only a few quantum numbers in their `.states` files as illustrated in Table 5: the polyad number P, vibrational angular momentum L, a polyad counting number N as well as $v_1^{\rm T}$, $v_2^{\rm T}$, and $v_3^{\rm T}$. The polyad number is estimated using the following simplified relation

$$P_i \approx \frac{\tilde{E}_i}{560\,\mathrm{cm}^{-1}} - L_i$$

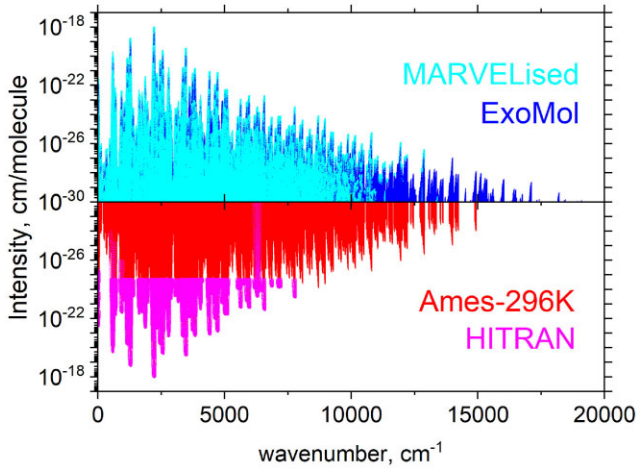

Figure 6. Illustration of the coverage of the MARVELized transitions in the room temperature ($T = 296$ K) TYM spectrum of $^{14}N_2{}^{16}O$ compared to the coverage in HITRAN (circles) and Ames-296K (sticks) (Huang et al. 2023). Where Ames-296K sticks are hidden by HITRAN points, their intensities closely follow HITRAN values as can be seen, e.g. in Fig. 4.

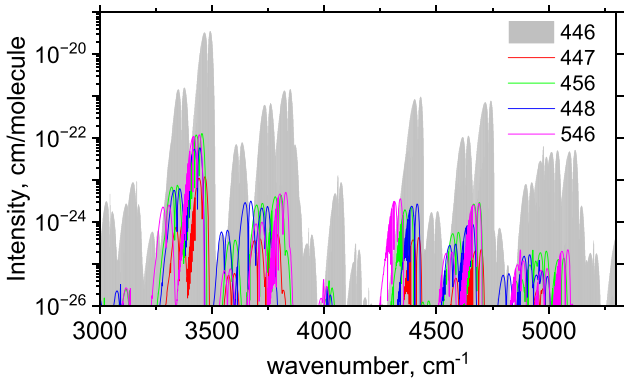

Figure 7. Absorption of isotopologues of N_2O at $T = 296$ K scaled with natural abundances. Isotopologues are denoted using the HITRAN shorthand label, see Table 2.

where $\tilde{E}_i$ is the energy term value of state i, 560 cm^{-1} is a rough estimate of the polyad quanta and L_i is the corresponding vibrational angular momentum.

Partition functions $Q(T)$ for all five isotopologues of N_2O were computed on a grid of 1 K from 0 to 2000 K and are available as `.pf` files from the ExoMol website. For $^{14}N_2{}^{16}O$, $Q(T)$ is illustrated in Fig. 2, where we also show the TIPS partition function from HITRAN 2020 (Gamache et al. 2021), which is essentially identical to that reported in Gamache et al. (2017). Our partition function is larger indicating better completeness at higher temperatures.

Temperature- and pressure-dependent molecular opacities of $^{14}N_2{}^{16}O$ based on the TYM line list have been generated using the ExoMolOP procedure (Chubb et al. 2021) for four exoplanet atmospheric retrieval codes: ARCiS (Min, Michiel et al. 2020), TauREx (Al-Refaie et al. 2021), NEMESIS (Irwin et al. 2008), and petitRADTRANS (Molliére et al. 2019) and available on the respective line list page of the species in question.

The TROVE input files are provided, with spectroscopic model used in TROVE calculations in the form of a TROVE input file, containing the potential energy and DMS parameters as well as the basis set specifications. This input file can be used with the FORTRAN code TROVE freely available from GitHub via www.github.org/exomol.[1]

Zero-pressure cross-sections of $^{14}N_2{}^{16}O$ are provided via the ExoMol cross-sections app. It can generate absorption cross-sections with the Doppler broadening line profile for temperatures from 100 to 2000 K covering the wavenumber range from 0 to 20000 cm^{-1} on a grid with a resolution of up to 0.01 cm^{-1} (Hill, Yurchenko & Tennyson 2013).

4 SPECTRA SIMULATIONS

Fig. 3 provides an overview of the spectrum of $^{14}N_2{}^{16}O$ at three temperatures, $T = 300$ K, $T = 1000$ K, and $T = 2000$ K from 0 to 20000 cm^{-1}, computed using the TYM line list. It is worth noting the profound temperature dependence of the band shapes in IR. In particular, the visual centres of the vibrational bands at $T = 2000$ K appear significantly red shifted comparing to the room temperature spectrum, which is highlighted in the inset of this figure showing the 1800–5000 cm^{-1} window.

In Figs 4 and 5, we present comparisons of TYM with the nitrous oxide line lists from other spectroscopic data bases. Fig. 4 compares room temperature ($T = 296$ K) absorption spectra of $^{14}N_2{}^{16}O$ generated using the N_2O line lists from Ames-296K (Huang et al. 2023), NOSL-296 (Tashkun & Campargue 2023), and N_2O HITRAN 2020 (Gordon et al. 2022) at low and high resolutions. A more extensive and detailed comparison of high-resolution spectra generated using these four line lists is given in Appendix B. There is a generally good agreement of ExoMol TYM with all three data bases, all the way up to the near infrared (NIR) region, where HITRAN' N_2O is absent, although there are also some differences in the weaker bands. The intensities of TYM are more similar to Ames-296K, which is expected due to the same dipole moment Ames-1 used in our work. The deviation from the NOSL-296 line list grows towards the NIR, where it is increasingly incomplete, especially above 10000 cm^{-1}, while Ames-296K only covers up to 15000 cm^{-1} (see Appendix B).

It should be noted, that the TYM line positions are shown before applying the MARVELization procedure, i.e. they are based on the original quality of the TYM spectroscopic model. This is important as it lends some trust to the quality of the predicted TYM spectra, which will need to be tested with the future experimental data.

Fig. 5 offers a similar comparison of TYM with hot line lists for N_2O, HITEMP (Hargreaves et al. 2019) and NOSD-1000 (Tashkun et al. 2016), where their absorption spectra of $^{14}N_2{}^{16}O$ at $T = 1000$ K are shown. Again, there is a generally good agreement between all three line lists, except for some cases of weak intensities as illustrated in the right display of this figure around 4800 cm^{-1}. The main disagreement is attributed to incompleteness of HITEMP and NOSD-1000 starting from NIR.

Fig. 6 illustrates the spectroscopic coverage of the MARVELized data in a TYM spectrum of $^{14}N_2{}^{12}O$ at $T = 296$ K and compares it to that of HITRAN and Ames-296K (Huang et al. 2023). HITRAN 2020 contains 33265 lines below 7800 cm^{-1}, our line list produces ~365 041 MARVELized lines, i.e. with experimentally accurate line positions, for $T = 296$ K and with intensities below 10^{-30} cm/molecule.

Fig. 7 illustrates the relative importance of the spectra of the isotopologues of N_2O at room temperature in an IR spectroscopic window, where the individual spectra are scaled by their natural

[1]See also the TROVE manual at https://docs.spectrove.org

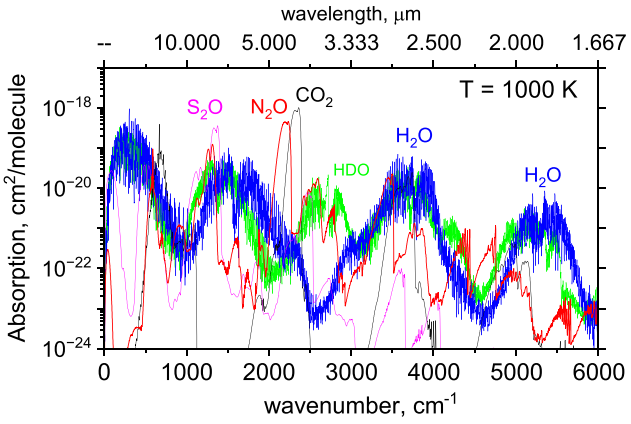

Figure 8. Absorption spectrum of N_2O at $T = 1000$ K overlaid with spectra of SO_2, CO_2, HDO, and H_2O using the ExoMol line lists due to Underwood et al. (2016), Yurchenko et al. (2020), Voronin et al. (2010), and Polyansky et al. (2018), respectively, and generated with a Gaussian line profile of HWHM = 2 cm^{-1}.

abundances taken from HITRAN. The minor isotopologues provide substantial contribution the overall spectrum of N_2O with intensities significantly larger than the HITRAN cutoff of 10^{-30} cm/molecule. Another illustration of the possible detectability of N_2O is presented in Fig. 8, where we overlay the absorption spectrum of $^{14}N_2{}^{12}O$ at $T = 1000$ K with absorption spectra of other atmospheric triatomic molecules, SO_2, CO_2, HDO, and H_2O. The strongest and most prominent absorption feature of N_2O, which is also in a water window, is at 4.5 μm, which is in a close vicinity from the 4.3 μm band of CO_2.

4.1 On the uncertainty of the calculated intensities

It is now a well-recognized problem that numerical noise associated with variational calculations can cause an overestimation of intensities of high-overtone transitions which has been discussed in a series of publications on diatomic molecules by Medvedev et al., see, e.g. Medvedev et al. (2015) and Medvedev & Ushakov (2022). Although there is no obvious indication of such plateaus forming at higher frequencies in our N_2O spectra in Figs 3–5 – they seem to show a nice exponential decrease of the intensities of the overtone bands, except perhaps the region of around 18000–20000 cm^{-1} – we decided to perform a more quantitative test of our intensities adapting the approach of suggested by Lodi & Tennyson (2012). To this end, we have computed a line list for N_2O using a different *ab initio* DMS by Schröder et al. (2015). The result of this test is illustrated in Fig. 9 (left display), where we show $T = 1000$ K cross-sections of $^{14}N_2{}^{16}O$ computed using two *ab initio* DMSs, 'Ames-1' and 'Schröder et al. (2015)' in conjunctions with our refined PES. The intensities generally agree up to about 13000 cm^{-1}, but less so above 13000 cm^{-1}. In fact, the 'DMS Schröder et al. (2015)' intensities appear to have a more natural exponential decline above 16000 cm^{-1}, where the 'DMS Ames-1' intensities have a slight increase of the 'Ames-1 intensities over 'DMS Schröder et al. (2015)' indicating a possible formation of a high-overtone plateau and could be a result of the deviation from the so-called Normal Intensity Distribution Law (Medvedev 2012). The analytical DMS representation of Schröder et al. (2015) has fewer parameters than that of Huang et al. (2023) (39 versus 572) and is presumably more stable for numerical errors at high overtones.

As a high resolution illustration, in the right display of Fig. 9, the corresponding $T = 296$ K line intensities of the ν_2 bands are shown, which we also compare to the HITRAN 2020 (Gordon et al. 2022) values. The 'DMS Schröder et al. (2015)' intensities (i.e. computed using our model and DMS by Schröder et al. 2015) appear to deviate from the HITRAN values by up to about 34 per cent. Analogous deviations were also found for the excited bending bands. Our choice to use the more recent DMS Ames-1 for the ExoMol line lists productions was influenced by this higher quality at lower wavenumbers.

5 CONCLUSION

In this work, ro-vibrational line lists for five main isotopologues of N_2O are presented. The line lists were computed using the variational approach TROVE employing a new empirical PES and an *ab initio* DMS from Schröder et al. (2015). The PES was generated via a fit to the experimentally derived energy term values of $^{14}N_2{}^{16}O$ from the MARVEL set by Tennyson et al. (2024) covering the rotational excitations up to $J = 80$. These energies were then used to improve the calculated values of $^{14}N_2{}^{16}O$ in the TYM line list. The

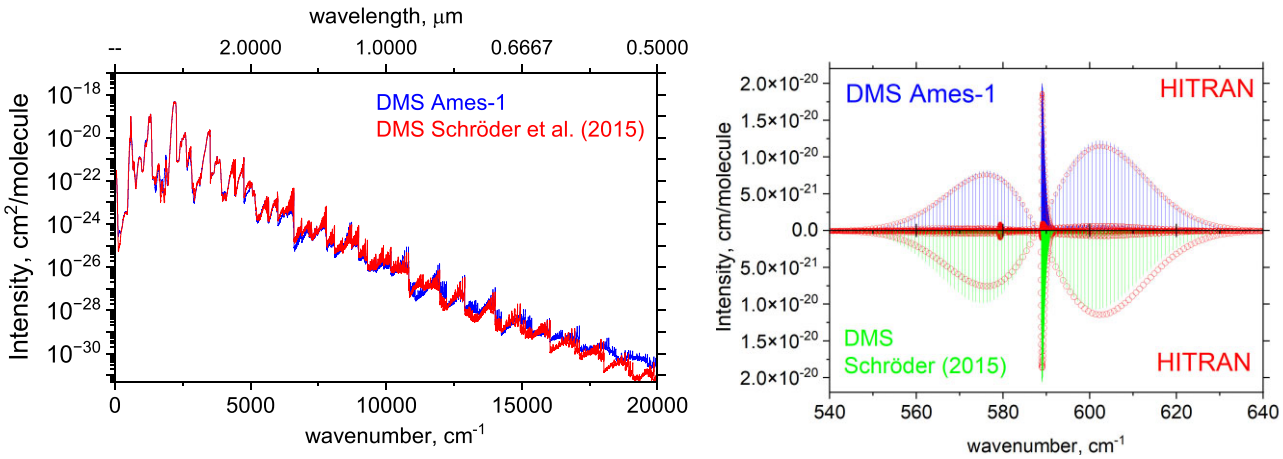

Figure 9. Intensities of $^{14}N_2{}^{16}O$ computed using two different *ab initio* DMSs, Huang et al. (2023) and Schröder et al. (2015) and our refined PES. Left: $T = 1000$ K cross-sections on a grid of 1 cm^{-1} using the Gaussian line profile with HWHM of 1 cm^{-1}. Right: ExoMol (sticks) and HITRAN (circles) line intensities at $T = 296$ K of the ν_2 band of $^{14}N_2{}^{16}O$.

line lists cover an extended wavenumber range up to 20000 cm^{-1} (> 0.5 μm) and the rotational excitations up to $J = 160$ with the estimated temperature coverage up to $T = 2000$ K. Owing to the MARVELization procedure used, we were able to predict over 300 000 new transitions of $^{14}N_2{}^{16}O$ with experimental accuracy. The line lists contain over a billion transitions each, ranging from 1.3 to 1.7 billion, depending on the isotopologue. At present only the parent $^{14}N_2{}^{16}O$ line list has been MARVELized; however, there are also extensive spectroscopic data available for the other isotopologues which are currently subject to a MARVEL analysis. Updated line lists using these results will be made available in due course.

In calculations, an artificial symmetry group C_{ns}(AEM) ($n = 18$; Mellor et al. 2021) was derived and used in TROVE calculations to facilitate the basis set construction.

ACKNOWLEDGEMENTS

This work was supported by the STFC project no. ST/Y001508/1 and by the European Research Council (ERC) under the European Union's Horizon 2020 research and innovation programme through Advance grant no. 883830. The authors acknowledge the use of the UCL Legion High Performance Computing Facility (Legion@UCL) and associated support services in the completion of this work. This work also used the DiRAC Data Intensive service (CSD3) at the University of Cambridge, managed by the University of Cambridge University Information Services and the DiRAC Data Intensive service (DIaL2) at the University of Leicester, managed by the University of Leicester Research Computing Service on behalf of the STFC DiRAC HPC Facility (www.dirac.ac.uk). The DiRAC services at Cambridge and Leicester were funded by BEIS, UKRI, and STFC capital funding and STFC operations grants.

DATA AVAILABILITY

The data underlying this article are available as part of the supporting information from the ExoMol data base at http://www.exomol.com. The TYM line list (states, transition, partition function files and a TROVE input specifying the spectroscopic model of N_2O) and opacities can be downloaded from www.exomol.com.[2] The refined PES of N_2O TYM used in this work is provided as part of the supplementary material, together with a comparison of the calculated TYM energies of $^{14}N_2{}^{16}O$ with the experimentally derived (MARVEL) energies (Tennyson et al. 2024).

REFERENCES

Al-Refaie A. F., Polyansky O. L., Ovsyannikov R. I., Tennyson J., Yurchenko S. N., 2016, MNRAS, 461, 1012
Al-Refaie A. F., Changeat Q., Waldmann I. P., Tinetti G., 2021, ApJ, 917, 37
Angerhausen D. et al., 2024, AJ, 167, 128
Bunker P. R., Jensen P., 1998, Molecular Symmetry and Spectroscopy, 2nd edn. NRC Research Press, Ottawa
Bunker P., Papoušek D., 1969, J. Mol. Spectrosc., 32, 419
Chubb K. L. et al., 2021, A&A, 646, A21
Cooley J. W., 1961, Math. Comp., 15, 363
Furtenbacher T., Császár A. G., Tennyson J., 2007, J. Mol. Spectrosc., 245, 115
Gamache R. R. et al., 2017, J. Quant. Spectrosc. Radiat. Transf., 203, 70
Gamache R. R. et al., 2021, J. Quant. Spectrosc. Radiat. Transf., 271, 107713
Gordon I. E. et al., 2022, J. Quant. Spectrosc. Radiat. Transf., 277, 107949
Grenfell J. L., 2017, Phys. Rep., 713, 1
Hargreaves R. J. et al., 2019, J. Quant. Spectrosc. Radiat. Transf., 232, 35
Hill C., Yurchenko S. N., Tennyson J., 2013, Icarus, 226, 1673
Hougen J. T., Bunker P. R., Johns J. W. C., 1970, J. Mol. Spectrosc., 34, 136
Huang X., Schwenke D. W., Lee T. J., 2014, J. Chem. Phys., 140, 114311
Huang X., Schwenke D. W., Lee T. J., 2021, Acc. Chem. Res., 54, 1311
Huang X., Schwenke D. W., Lee T. J., 2023, Mol. Phys., 122, e2232892
Irwin P. G. J. et al., 2008, J. Quant. Spectrosc. Radiat. Transf., 109, 1136
Lodi L., Tennyson J., 2012, J. Quant. Spectrosc. Radiat. Transf., 113, 850
López-Puertas M., Funke B., Bermejo-Pantale'on D., von Clarmann T., Stiller G. P., Grabowski U., Höpfner M., 2007, Geophys. Res. Lett., 34, L02825
Medvedev E. S., 2012, J. Chem. Phys., 137, 174307
Medvedev E. S., Ushakov V. G., 2022, J. Quant. Spectrosc. Radiat. Transf., 288, 108255
Medvedev E. S., Meshkov V. V., Stolyarov A. V., Gordon I. E., 2015, J. Chem. Phys., 143, 154301
Mellor T. M., Yurchenko S. N., Jensen P., 2021, Symmetry, 13, 548
Min Michiel, Ormel Chris W., Chubb Katy, Helling Christiane, Kawashima Yui, 2020, A&A, 642, A28
Molliére P., Wardenier J. P., van Boekel R., Henning T., Molaverdikhani K., Snellen I. A. G., 2019, A&A, 627, A67
Noumerov B. V., 1924, MNRAS, 84, 592
Polyansky O. L., Kyuberis A. A., Zobov N. F., Tennyson J., Yurchenko S. N., Lodi L., 2018, MNRAS, 480, 2597
Rothman L. S. et al., 2010, J. Quant. Spectrosc. Radiat. Transf., 111, 2139
Sagan C., Thompson W. R., Carlson R., Gurnett D., Hord C., 1993, Nature, 365, 715
Schröder B., Sebald P., Stein C., Weser O., Botschwina P., 2015, Z. Phys. Chem., 229, 1663
Schwieterman E. W. et al., 2018, Astrobiology, 18, 663
Schwieterman E. W. et al., 2022, ApJ, 937, 109
Tashkun S. A., Campargue A., 2023, J. Quant. Spectrosc. Radiat. Transf., 295, 108417
Tashkun S. A., Perevalov V. I., Lavrentieva N. N., 2016, J. Quant. Spectrosc. Radiat. Transf., 177, 43
Teffo J., Perevalov V., Lyulin O., 1994, J. Mol. Spectrosc., 168, 390
Tennyson J., Hill C., Yurchenko S. N., 2013, AIP Conf. Proc. Vol. 1545, Eighth International Conference on Atomic and Molecular Data and their Applications. Am. Inst. Phys., New York, p. 186
Tennyson J., Furtenbacher T., Yurchenko S. N., Császár A. G., 2024, J. Quant. Spectrosc. Radiat. Transf., 316, 108902
Tinetti G. et al., 2012, Exp. Astron., 34, 311
Tyuterev V. G., Tashkun S. A., Schwenke D. W., 2001, Chem. Phys. Lett., 348, 223
Underwood D. S., Tennyson J., Yurchenko S. N., Huang X., Schwenke D. W., Lee T. J., Clausen S., Fateev A., 2016, MNRAS, 459, 3890
Vasquez M., Schreier F., Garcia S. G., Kitzmann D., Patzer B., Rauer H., Trautmann T., 2013, A&A, 549, A26
Voronin B. A., Tennyson J., Tolchenov R. N., Lugovskoy A. A., Yurchenko S. N., 2010, MNRAS, 402, 492
Waalkens H., Jung C., Taylor H. S., 2002, J. Phys. Chem. A, 106, 911
Yurchenko S. N., Mellor T. M., 2020, J. Chem. Phys., 153, 154106
Yurchenko S. N., Thiel W., Jensen P., 2007, J. Mol. Spectrosc., 245, 126
Yurchenko S. N., Yachmenev A., Ovsyannikov R. I., 2017, J. Chem. Theory Comput., 13, 4368
Yurchenko S. N., Mellor T. M., Freedman R. S., Tennyson J., 2020, MNRAS, 496, 5282
Ziurys L. M., Apponi A. J., Hollis J. M., Snyder L. E., 1994, ApJ, 436, L181

SUPPORTING INFORMATION

Supplementary data are available at *MNRAS* online.

N20_MARVEL-TROVE.txt

Please note: Oxford University Press is not responsible for the content or functionality of any supporting materials supplied by the authors.

[2] https://exomol.com/data/molecules/N2O/14N2-16O/TYM

Any queries (other than missing material) should be directed to the corresponding author for the article.

APPENDIX A: ARTIFICIAL SYMMETRY

The internal vibrational modes r_1, r_2, and ρ used in our model are effectively coordinates of a bent molecule. These span two irreducible representations, Σ^+ and Σ^- (or A' and A'') of $C_{\infty v}$(M) (isomorphic to C_s) and do not reflect the symmetry properties of a linear molecule. An alternative symmetry description of vibrational and rotational functions of a linear molecule is offered by the symmetry group $C_{\infty v}$(EM) (Bunker & Papoušek 1969) spanning much more versatile irreducible representations with Σ, Π, Δ, Φ,... for L= 0, 1, 2, 3,... and K= 0, 1, 2, 3, for the vibrations and rotations respectively. Their advantage of this description is this direct and unique association of the indices L and K with irreducible representations of $C_{\infty v}$(EM), with all the efficient and useful properties. Here we introduce the artificial symmetry group C_{ns}(AEM) associated with the basis set of a bent molecule but possessing this property of the linear molecule group $C_{\infty v}$(EM) where the corresponding irreps are uniquely classified by indices L or K.

In order construct the irreducible representations of the finite artificial extended molecular symmetry group C_{ns}(AEM), we follow the D_{nh}(AEM) methodology by Mellor et al. (2021) developed for symmetric linear molecules. The group in question is thus defined by

$$C_{ns}(\mathrm{AEM}) = C_s \otimes \mathbf{Z}_2 \underbrace{\otimes \ldots \otimes}_{n-3} \mathbf{Z}_2,$$

where $\mathbf{Z}_2$ is the cyclic group of order 2 and, therefore, it consists of the set {0, 1} with addition modulo 2. The integer n depends on the value of $L_{\max}$ and is given by

$$n = \lceil \log_2 2(L_{\max} + 1) \rceil, \tag{A1}$$

where $\lceil\rceil$ rounds up and $L_{\max}$ is the maximum value of L (or k). For example, the character table of C_{4s}(AEM) is given in Table 1. This corresponds to $L_{\max} = 3$ and the number of irreps in the group equals the number necessary for the reassignment of the bending and rotational functions, though this is not true in general because of the rounding applied in equation (A1). In either case, the extra irreps are needed as seen below.

When combining bending function that transform as Γ^L_{bend} of C_{ns}(AEM) with rotational functions which transform as Γ^K_{rot}, their product should transform as $\Gamma^L_{\mathrm{bend}} \times \Gamma^K_{\mathrm{rot}} = (\Gamma_{\mathrm{bend}} \times \Gamma_{\mathrm{rot}})^m$ for some $m \neq 0$ if $l \neq k$. If $L = K$, then they should transform as $\Gamma^L_{\mathrm{bend}} \times \Gamma^K_{\mathrm{rot}} = (\Gamma_{\mathrm{bend}} \times \Gamma_{\mathrm{rot}})^0$. For example, $A'^4 \times A''^4$ should be A''^0.

The symmetry group C_{ns}(AEM) for a general n is implemented into TROVE where the effects of the group operations on the coordinates is as follows: all operations leave the vibrational coordinates invariant; the E^a operations (in the notation of Table 1) leave the rotational functions invariant while the σ^a operation has the same effect as the σ^0 operation.

APPENDIX B: ROOM TEMPERATURE SPECTRUM OF $^{14}N_2{}^{16}O$

Figs. B1 and B2 provide a detailed comparison of $T = 296$ K absorption spectra of $^{14}N_2{}^{16}O$ in 9 spectroscopic windows computed using four line lists, TYM, HITRAN2020' N_2O (Gordon et al. 2022), NOSL-296 (Tashkun & Campargue 2023), and Ames-296K (Huang et al. 2023). Left display: a log-scale illustration of the coverage of TYM, Ames-296K and NOSL-296 using a Gaussian line profile with HWHM of 1 cm^{-1} was used. HITRAN line intensity values are indicated by red empty circles (in the upper and lower displays), NOSL-296 values are with dark blue circles (bottom displays), Ames-296K lines are given by green sticks (bottom display), and TYM lines are shown by blue sticks in the upper displays. The TYM line positions are given by the TROVE values before the MARVELization procedure in order to illustrate the quality of the refined spectroscopic model used in the line list calculations.

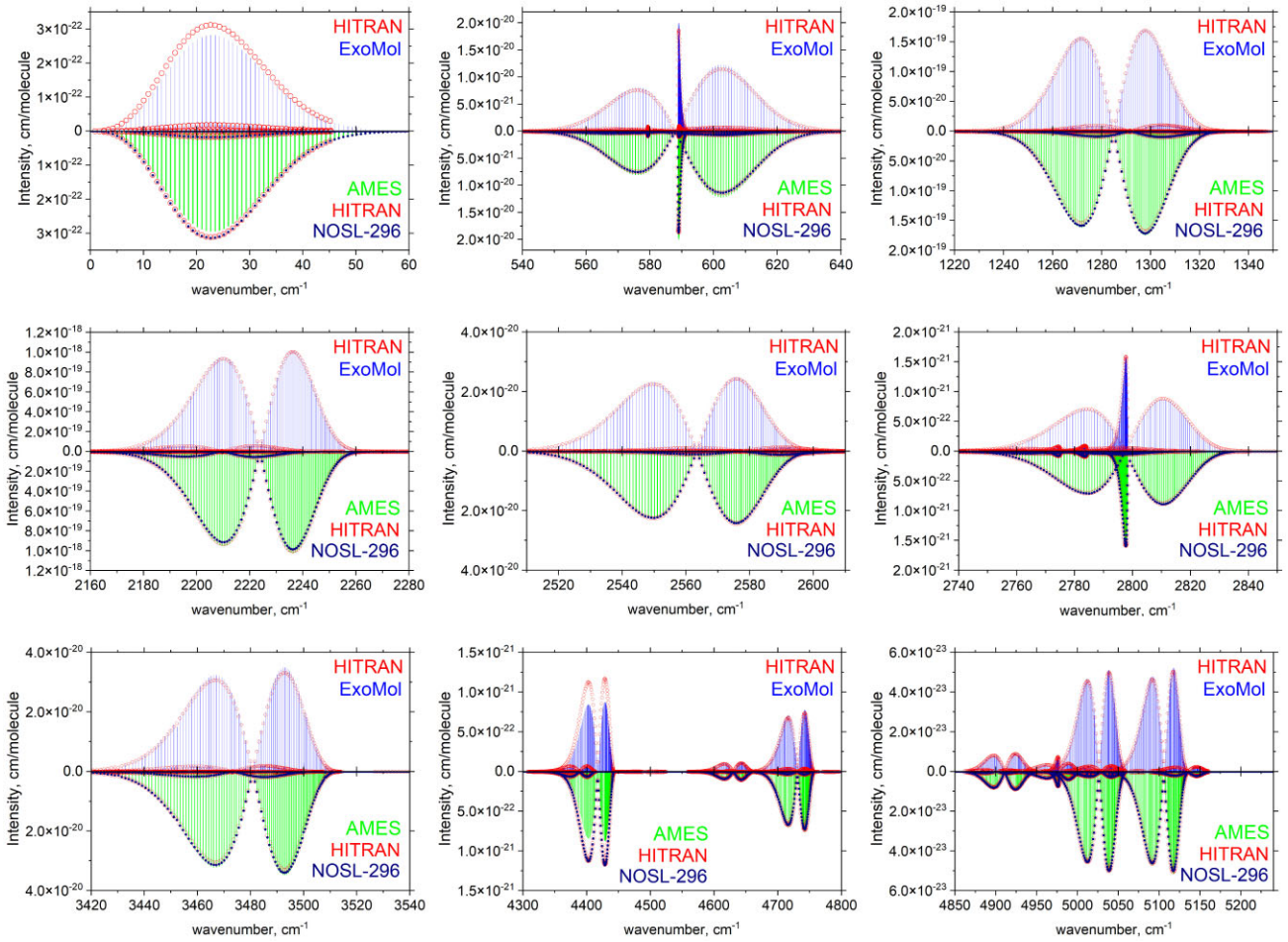

Figure B1. Comparison of $^{14}N_2{}^{16}O$ $T = 296$ K absorption intensities (cm/molecule) computed using four line lists, TYM (ExoMol), HITRAN 2020 (Gordon et al. 2022), NOSL-296 (Tashkun & Campargue 2023), and Ames-296K covering the range 0–5200 cm^{-1}: HITRAN (empty circles), NOSL-296 (circles), Ames-296K (sticks), and TYM (sticks).

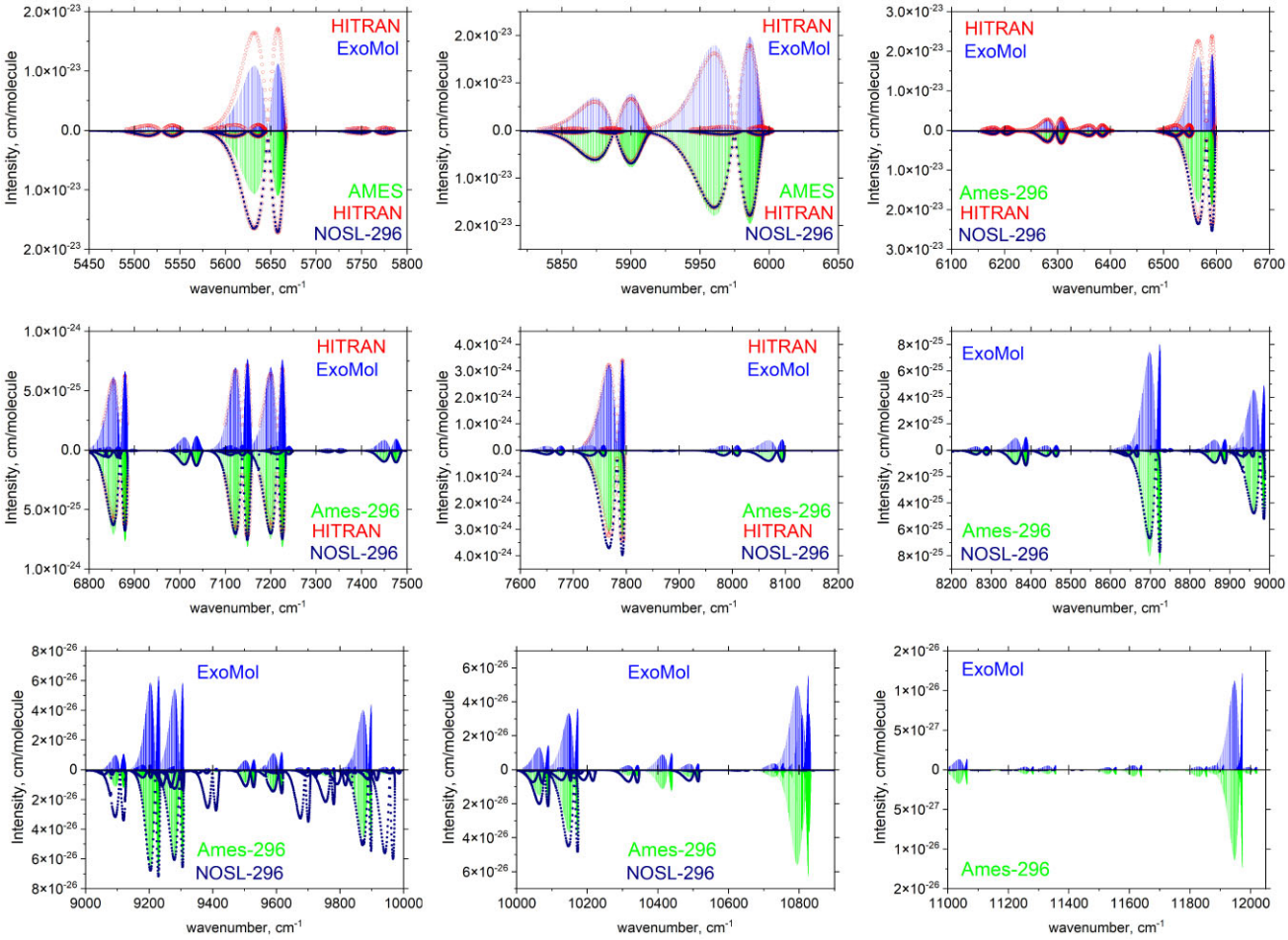

Figure B2. Comparison of $^{14}N_2{}^{16}O$ $T = 296$ K absorption intensities (cm/molecule) computed using four line lists, TYM (ExoMol), HITRAN 2020 (Gordon et al. 2022), NOSL-296 (Tashkun & Campargue 2023), and Ames-296K covering the range 5200–12000 cm^{-1}: HITRAN (empty circles), NOSL-296 (circles), Ames-296K (sticks), and TYM (sticks).

This paper has been typeset from a TEX/LATEX file prepared by the author.